# First-principles study of bismuth films at transition-metal grain boundaries

Qin Gao and Michael Widom
*Department of Physics, Carnegie Mellon University, Pittsburgh, Pennsylvania 15213, USA*
(Received 11 December 2013; revised manuscript received 9 September 2014; published 10 October 2014)

Recent experiments suggest that Bi impurities segregate to form bilayer films on Ni and Cu grain boundaries (GBs) but do not segregate in Fe. To explain these phenomena, we study the total energies of Bi films on transition-metal (TM) $\Sigma3(111)$ and $\Sigma5(012)$ GBs using density functional theory. Our results agree with the observed stabilities. We propose a model to predict Bi bilayer stability at Ni GBs which suggests that Bi bilayer is not stable on (111) twist CSL GBs but is stable in most (100) twist CSL GBs. We investigate the interaction and bonding character between Bi and TMs to explain the differences among TMs based on localization of orbitals and magnetism, as well as evaluating the contribution of interfacial phonons at high temperature.

DOI: 10.1103/PhysRevB.90.144102 PACS number(s): 62.20.mj, 61.72.Mm, 71.20.Be, 73.61.At

## I. INTRODUCTION

Segregation at grain boundaries (GBs) affects various properties of polycrystals such as grain growth [1,2], liquid metal embrittlement (LME) [3,4], and corrosion [5,6]. However, the exact segregated structures, and hence the underlying mechanisms at atomic level, are far from being fully revealed. As a generalization of Gibbs' definition of phase, the new concept "complexion" was proposed to describe thermodynamically stable interfacial structures [7,8].

Recently, Dillon-Harmer complexions [9,10] were discovered in metallic systems Bi-Ni [11] and Bi-Cu [12], which could possibly explain the long standing puzzle of LME. In these experiments, Bi formed bilayer films ubiquitously in Ni at general orientation GBs around the penetration tip. In contrast, a clean low energy Ni grain boundary was found. Bi also formed bilayer films at Cu GBs around the penetration tip. However, the bilayer films were only observed close to the tip than at Ni GBs indicating bilayer films were stable over a much narrower Bi chemical potential window. Similar to Ni, Bi did not segregate at low energy Cu GBs. A study of Fe revealed no Bi films [13].

A recent theoretical study [14] of Bi at Ni and Cu(111) twist and $\Sigma5(310)$ GBs found the Bi bilayer enthalpy of formation on $\Sigma5(310)$ is negative, which indicates thermodynamic stability, while on (111) twist GBs it is positive. The authors proposed that bilayers are more stable than monolayers based on interaction strength between Bi and Ni layers and an electric dipole generated in the Bi bilayer on (111) twist GB. However, neither the origin of different segregation behavior of Bi on Ni compared with Cu, nor the relative stability of bilayer and trilayer films, was discussed. Moreover, a detailed study of the film structure, registry, and bonding character is needed.

In this paper, we present a first-principles study of Bi films on low energy $\Sigma3(111)$ and high energy $\Sigma5(210)$ transition metal GBs. Our study explains bilayer film formation on Ni and Cu high energy GBs and its absence on Fe GBs (see Appendix 1 for Fe). Moreover, we discover a nonmonotonic trend of Bi bilayer stability at 3*d* transition metals Co, Ni, and Cu. We explain this trend based on competing effects of orbital localization and magnetization, and confirm this analysis with crystal orbital Hamilton population (COHP) [15,16] calculations. By exploiting the weak Bi interlayer interaction, we propose a model that can be used to predict Bi bilayer stability on various Ni GBs with relatively simple surface calculations. We discuss the temperature effect and the effect of Bi bilayer on embrittlement.

## II. METHODS

Our calculation methods are similar to our study of Bi on Ni(111) [17], namely PAW potentials [18,19] in the PBE [20] generalized gradient approximation with default energy cutoffs using VASP [21,22]. To find stable structure at GBs, we first study Bi structures on free surfaces. For Bi on TM(111) and (120), we construct models based on four and six metal layers normal to the surface respectively with Bi films on one side. We choose the $\Sigma3(111)$ twist and the $\Sigma5(012)$ tilt GBs as representative low energy and high energy GBs, respectively. $\Sigma3(111)$ is formed by cleaving the bulk along the (111) plane, rotating one grain around [111] by 60°, and rejoining the two parts [23]. $\Sigma5(012)$ is formed by cleaving the bulk along the (012) plane, rotating one grain around [100] by 53.1°, and rejoining the two parts after removing overlapping atoms (see Fig. 1).

For Bi on $\Sigma3(111)$ GBs we stack six layers of metal with periodic boundary conditions and rotate three layers relative to the other three, thus creating the GBs. Then we insert our Bi film at one GB, leaving the other bare. To reduce computational complexity, the segregated structures at $\Sigma5(012)$ GBs are calculated with six layers TM at each side of the Bi films and terminated by bare TM surfaces with vacuum at both sides. Convergence with respect to the number of Ni layers is documented in Appendix 2. The $\Sigma5(120)$ GB plane is shown in Fig. 1. Later on, we refer to the blue solid cell as $(1 \times 1)$, green dashed cell as $(3 \times 1)$, and cyan dash-dotted cell as $(1 \times 4)$. To analyze interaction strength and bonding character, we perform COHP calculations which evaluate matrix elements of the total energy between pairs of atomic orbitals on neighboring atoms. The differential (dCOHP) reveals the bonding and antibonding orbitals, while the integral up to the Fermi energy (iCOHP) measures the bond strength.

## III. RESULTS AND DISCUSSION

### A. Film stability

Our calculated GB energies $E_{GB}$ are shown in Table I, and agree well with prior literature.

 

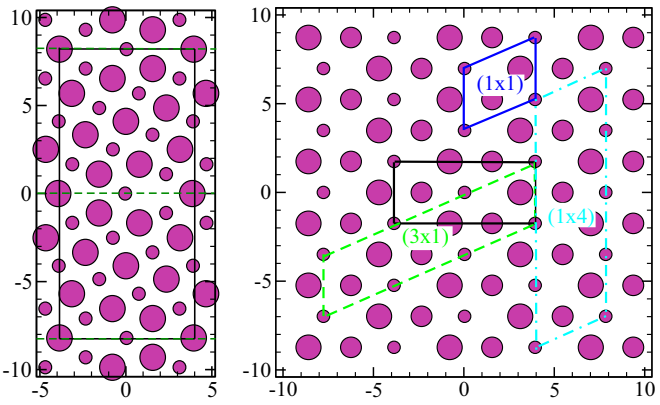


FIG. 1. (Color online) Left: side view of our Σ5(012) GB. The black cell is our unit cell. The dashed green lines are GB planes. Right: top view of Σ5(012) GB plane. Three layers of atoms are shown. The black solid cell is the orthorhombic unit cell we use to calculate Σ5(012) GB energies. Atom size indicates depth (large below small). Units are Å.

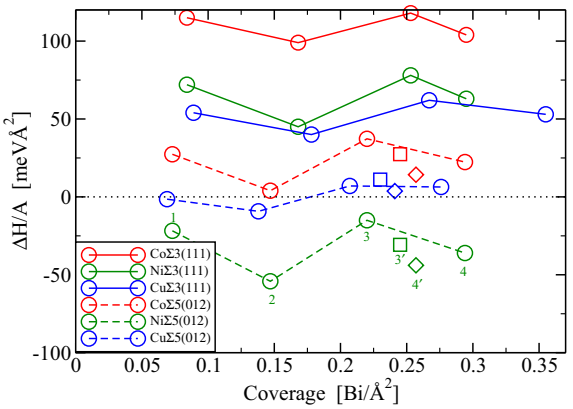


FIG. 2. (Color online) Enthalpies of Bi films at Σ3(111) and Σ5(012) GBs. Solid lines connect Bi films on Σ3(111) GBs. Films of 1–3 layer thickness (labeled 1–3) have 4 Bi atoms per layer while the four-layer films contain 4 Bi atoms per layer in layers adjacent to Ni but 3 Bi per layer in the middle two layers [17] for Ni and Co. Films for Cu have 2 Bi per layer. Dashed lines connect Bi films in (1 × 1) cells of Σ5(120) GBs. Red, green, and blue colors indicate Co, Ni, and Cu, respectively. Square points (labeled as 3′) stand for trilayer films in (3 × 1) cells of Σ5(120) GBs with denser middle layer [4 Bi in (3 × 1) cell]. Diamond points (labeled as 4′) stand for four layer films in (1 × 4) cells of Σ5(012) GBs with the in-plane density of the middle bilayer similar to bulk Bi [3 Bi in a (1 × 4) cell].

For Bi on the Ni(111) surface, we found a four-atom Bi monolayer on a (3 × 3) surface cell is stable over a wide Bi chemical potential [17], and the same holds true for Co. For Bi on the Cu(111) surface, two-atom Bi monolayer on a [2012] cell is stable, which agrees with experimental observation [27]. On TM(120) surfaces, Bi sitting on the valley sites of (1 × 1) cells [28] are stable over a wide range of chemical potential.

We then study various Bi films at GBs. To compare the stability of these films, we calculate the enthalpy of formation, which is defined as

$$\Delta H/A = \left[E_{\text{tot}} - E^{\text{TM}}_{\text{slab}} - E^{\text{Bi}}_{\text{bulk}} N_{\text{Bi}}\right]/A, \qquad (1)$$

where $E_{\text{tot}}$ is the energy of a TM slab containing GB segregated by Bi, $E^{\text{TM}}_{\text{slab}}$ is the energy of a TM slab containing a bare GB, $E^{\text{Bi}}_{\text{bulk}}$ is the Bi bulk energy, and $A$ is the GB area. Figure 2 shows our enthalpies of formation. On the low energy Σ3(111) GBs, the enthalpies of Bi film formation are all large and positive, which suggests that Bi does not form stable films at these GBs. This is expected since the Σ3(111) GB differ from bulk only by a low energy stacking fault. It is energetically unfavorable to cut the strong bulklike metal bonds and replace them by bonds with Bi. These results agree with the experimental observation [11,12] of bare Ni and Cu low energy GBs near the Bi penetration tip. At the high energy Σ5(120) GB, $\Delta H$ is reduced for all TM. At Co Σ5(120) GB, $\Delta H$ remains positive suggesting all films are unstable. For Ni, all Bi films have negative $\Delta H$, which means Bi penetration is favorable for all these films. Moreover, bilayer Bi is most favorable, with lower enthalpy of formation than monolayer and trilayer. For Cu, Bi monolayer and bilayer film have negative enthalpies of formation. The bilayer preference is less pronounced than on Ni. Overall, the enthalpy of formation is less negative on Cu than on Ni, which indicates interfacial films are less favorable in the case of Cu.

TABLE I. GB energies; units are eV/Å$^2$. The energy conversion factor is 1 eV/Å$^2$ = 16 J/m$^2$. Values from other studies are in parentheses. Note the Co Σ3(111) GB energy is negative because the $T = 0$ K state is HCP rather than the high-$T$ FCC that we choose to compare with.

| GB | Co | Ni | Cu |
|---|---|---|---|
| Σ 3(111) | −0.0016 | 0.0028 (0.0027 [24]) | 0.0001 (0.0014 [24]) |
| Σ 5(120) | 0.080 | 0.077 (0.089 [25]) | 0.055 (0.059 [26]) |

To further illustrate the stability of Bi films at Σ5(120) GBs, we calculate the GB free energy. From equilibrium thermodynamics, the most stable structure at a certain Bi chemical potential minimizes the GB free energy $\gamma$ [29],

$$\gamma = [\Delta H - \Delta\mu_{\text{Bi}} N_{\text{Bi}}]/A, \qquad (2)$$

where $\Delta\mu_{\text{Bi}} \equiv \mu_{\text{Bi}} - E^{\text{Bi}}_{\text{bulk}}$ is the Bi relative chemical potential. Note that $\Delta\mu_{\text{Bi}} = 0$ corresponds to the chemical potential of bulk Bi.

As shown in Fig. 3, the stable sequence at Co Σ5(120) GB goes from a bare GB plane directly to an infinite height bulklike film at $\Delta\mu_{\text{Bi}} = 0$ eV. In contrast, a Bi bilayer film is stable for $-0.37 < \Delta\mu_{\text{Bi}} < 0$ eV on Ni Σ5(120) GB and for $-0.067 < \Delta\mu_{\text{Bi}} < 0$ eV on Cu Σ5(120) GB. Bi films are thus not stable on Co Σ5(120) GB. Moreover, the bilayer films are stable over a much wider chemical potential window on Ni than Cu Σ5(120) GB, which is consistent with the experimental observations [11,12].

Studying other bilayer films with different registry and coverage, it turns out the valley site of a missing Ni atom is a strong Bi adsorption site. For structures with Bi density smaller than the (1 × 1) film, all Bi atoms relax into valley sites. The (1 × 1) film (see Fig. 4) is more stable than these films due to the energy gain by putting more Bi at the remaining empty valley

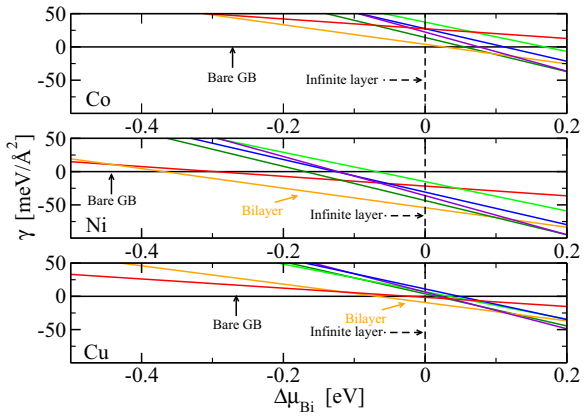


FIG. 3. (Color online) GB free energy of Bi films at Co, Ni, Cu Σ5(120) GBs, respectively, top to bottom. The black solid lines stand for bare GBs, while the black dashed lines stand for infinite bulklike Bi films. Other lines are for different Bi films, with stable bilayer labeled.

sites. With Bi density larger than the $(1 \times 1)$ film, Bi atoms in each layer bond with each other in the unfavorable metallic form and also leave some empty valley sites which weakens the bonds with Ni. Both these effects destabilize such films.

Trilayer films are unfavorable at all GBs, again because of the bonding character of Bi. Bulk Bi has the common $\alpha$-As group-V semimetal (strukturbericht A7, Pearson *hR2*) with rhombohedral space group $R\bar{3}m$ forming a bilayer structure. Each Bi atom has strong covalent bonds with three intrabilayer neighbors at the distance of 3.1 Å and bonds weakly with three interbilayer neighbors at 3.5 Å. The trilayer films contain a chemically adsorbed monolayer on each side of the GB plus a monolayer of atoms in between that forms metallic bonds. The four layer structure has a bilayer film similar to the bulk structure between the strong adsorbed monolayer films. Thus bilayer films and four layer films are more favorable than trilayer films. The observed trilayer Bi film at Ni GB near the penetration tip is thus indeed predicted to be a metastable structure as inferred in Ref. [11].

### B. Thermodynamic model

The Bi interlayer interaction is weak in the bilayer films at both Ni Σ3(111) and Σ5(120) GBs, with bond lengths

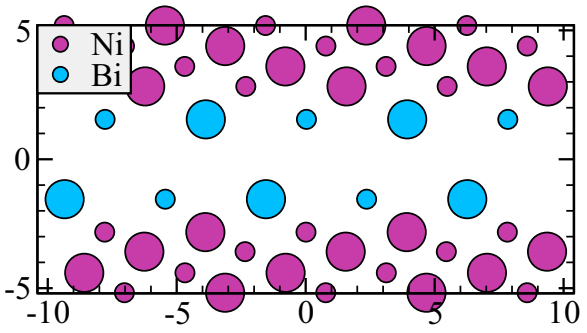


FIG. 4. (Color online) Relaxed bilayer Bi films at $(1 \times 1)$ cell of Ni Σ5(120) GB. Only Ni atoms close to Bi are shown. Atom size indicates depth (large below small). Units are Å.

TABLE II. Calculated input quantities for the enthalpy model [Eq. (3)]. Predicted $E_{GB}^{min}$ values for GB with the same surface plane (i.e., $a = b$) at two sides. The energy units are eV/Å$^2$. The Bi monolayer structure on Ni(100) surface is the $c(2 \times 2)$ structure as observed in experiment [30].

| Surface | $E_{surf}$ | $\Delta H_{ML}$/A | $E_{GB}^{min}$ |
|---|---|---|---|
| (111) | 0.118 | −0.090 | 0.056 |
| (001) | 0.137 | −0.122 | 0.030 |
| (120) | 0.150 | −0.133 | 0.034 |

around 3.9 Å and 4.2 Å, respectively, which are larger than the weak Bi-Bi metallic bond. In experiment, the observed Bi layer spacing is $3.9 \pm 0.6$ Å. Based on these observations, we propose a model to calculate the enthalpy of formation of Bi bilayer at Ni GBs with bare GB energies and surface adsorptions, by neglecting the Bi interlayer interaction,

$$\Delta H/A \approx E_{surf}^{a} + \Delta H_{ML}^{a}/A + E_{surf}^{b} + \Delta H_{ML}^{b}/A - E_{GB}, \tag{3}$$

where $E_{surf}^{a}$ and $E_{surf}^{b}$ are the surface energies of Ni surfaces $a$ and $b$ adjacent to the GB plane and $\Delta H_{ML}^{a}$ and $\Delta H_{ML}^{b}$ are the enthalpies of formation of Bi monolayers on Ni surfaces $a$ and $b$. The first four terms represent the excess energy per area with bilayer intercalation. $E_{GB}$ is the excess energy per area without intercalation. The values are shown in Table II. We define $E_{GB}^{min}$ as the minimum energy of GB consisting of surfaces $a$ and $b$ such that formation of Bi bilayer is energetically favorable, i.e., for which $\Delta H/A \leqslant 0$. Hence

$$E_{GB}^{min} \approx E_{surf}^{a} + \Delta H_{ML}^{a}/A + E_{surf}^{b} + \Delta H_{ML}^{b}/A. \tag{4}$$

Results of this model are given in Table III.

The enthalpies of formation from model predictions ($\Delta H^{model}$) and direct calculations ($\Delta H^{calc}$) are within

TABLE III. Model and calculated Ni GB energies and Bi bilayer enthalpies of formation at different Ni GBs. Work of separation for bare and Bi bilayer segregated GBs is shown on the right. The energy units are eV/Å$^2$. The Σ7(111) GB is made by twisting the one side of bulk Ni by 21.8° around the [111] axis with (111) as GB plane. The resulting GB cell is [3-112] as defined in [31] on which Bi favors three atoms per layer. The Σ5(100) GB is made by twisting one side of bulk Ni by 36.9° around the [001] axis with (001) as GB plane. The general GB (111)/(100) is constructed with $a$ = (111) and $b$ = (100) planes with a $(3 \times 3)$ surface cell at the $a$ side and a [2-213] surface cell (following the notation of [31]) at the $b$ side. Unlike the CSL GBs, this general GB $\Delta H^{calc}$ is greater than $\Delta H^{model}$ due to strain of the Ni cells (around 5%). This artificial strain introduced by forcing the two weakly interacting grains to share a common small cell makes the direct calculation inaccurate.

| GB | $E_{GB}$ | $\Delta H^{model}$/A | $\Delta H^{calc}$/A | $W_{sep}^{bare}$ | $W_{sep}$ | Reduction |
|---|---|---|---|---|---|---|
| Σ3(111) | 0.003 | 0.053 | 0.045 | 0.235 | 0.009 | 96.2% |
| Σ7(111) | 0.029 | 0.027 | 0.023 | 0.209 | 0.009 | 95.7% |
| Σ5(100) | 0.064 | −0.034 | −0.037 | 0.208 | 0.007 | 96.6% |
| Σ5(120) | 0.077 | −0.043 | −0.054 | 0.220 | 0.010 | 95.5% |
| (111)/(100) | 0.055 | −0.012 | −0.004 | 0.207 | 0.004 | 98.0% |

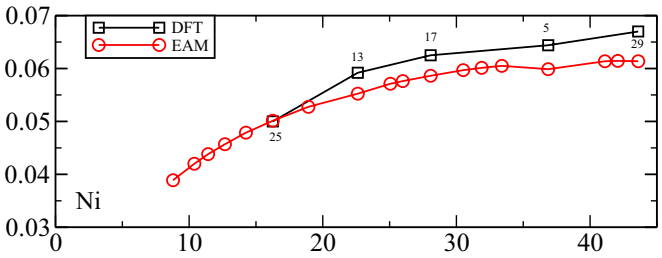


FIG. 5. (Color online) Grain boundary energies calculated by DFT compared with the embedded atom method (EAM) for Ni and Cu. The EAM data is taken from [32]. Numbers shown in the figure are the Σ values of those CSL GBs. For both metals, the results show similar trends and differ by less than 0.005 eV/Å$^2$.

0.01 eV/Å$^2$, and slightly exceed the direct calculations because we neglect the interaction between Bi bilayers which lower the total energy. This model thus accurately predicts Bi bilayer enthalpies of formation, while being easier to calculate than direct Bi at Ni GBs.

Approximate energies for many bare GBs can be obtained from embedded atom method (EAM) calculations [33]. Direct comparison between DFT and EAM bare GB energies is shown in Fig. 5. The differences are small and within 0.005 eV/ Å$^2$, and thus do not strongly effect the model prediction. Based on the EAM bare GBs, our model predicts that Bi bilayer enthalpies of formation are positive on all Ni(111) CSL twist GBs, but are negative on (100) CSL twist GBs for rotation angles between 10° and 45°. Moreover, for GBs with different adjacent surfaces (i.e., $a \neq b$) that are not commensurate with each other, model predictions that avoid artificial strain might be more accurate than affordable direct calculations. An example is shown in Table III. This model could easily be generalized to other polycrystalline materials providing the interlayer interaction of segregated films is small.

### C. Embrittlement and differences among TMs

Ni GBs are severely embrittled by Bi bilayer segregation. In Table III, we show the work of separation (defined as $W_{sep} = 2E_{surf} - E_{GB}$, the work needed to separate the GB [34]) at several bare and Bi segregated GBs. In all these GBs, $W_{sep}$ is reduced by more than 95% due to the weak interaction between Bi layers [14].

TABLE IV. (012) surface energy, Bi monolayer enthalpies of formation, integrated COHP (iCOHP) energies of Bi-TM bond, TM-TM bond near to Bi (a), and TM-TM bond away from impurities (b). The energy units are eV/bond for the iCOHP energies.

| | Co (nonmag) | Co (mag) | Ni (nonmag) | Ni (mag) | Cu Cu |
|---|---|---|---|---|---|
| $E_{surf}$ (eV/Å$^2$) | 0.193 | 0.164 | 0.152 | 0.150 | 0.100 |
| $\Delta H$ (eV/Å$^2$) | −0.160 | −0.118 | −0.152 | −0.133 | −0.070 |
| iCOHP(Bi-TM) | −1.75 | −1.63 | −1.77 | −1.75 | −1.33 |
| iCOHP(TM-TM)[a] | −1.38 | −1.32 | −1.13 | −1.13 | −0.43 |
| iCOHP(TM-TM)[b] | −1.17 | −1.16 | −0.85 | −0.83 | −0.66 |

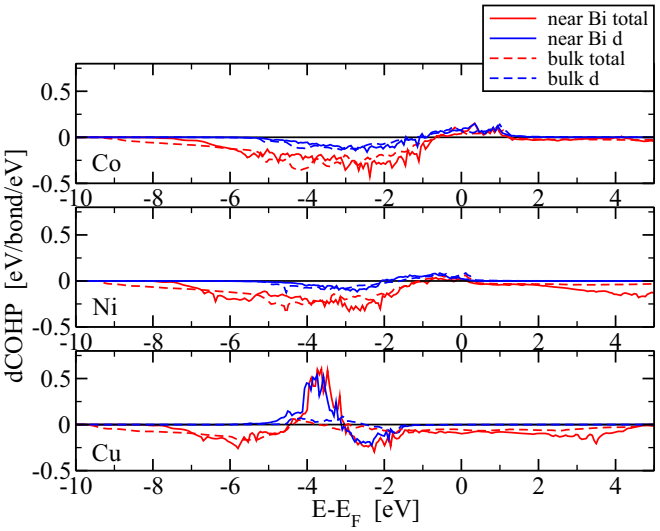


FIG. 6. (Color online) Differential COHP of metal-metal interaction in the bulk and near to Bi. Negative is bonding while positive is antibonding. The Ni and Co results are the summation of two spin components. The dashed green line is the $x$ axis. The zero in $x$ axis is the Fermi energy.

The differences of Bi interactions among these three transition metal GBs can be understood with a combination of localization of TM electron orbitals and magnetism. With increasing of atomic number from Co to Ni and to Cu, the 3$d$ orbital becomes more localized, and thus the interactions between TMs and with Bi decreases. For example, shown in Table IV the (012) surface energies $E_{surf}$ and Bi monolayer $\Delta H/A$ on (012) surface diminish for Co, Ni, and Cu, respectively, in nonmagnetic calculation. With magnetism, Co and Ni(012) $E_{surf}$ decrease further due to increasing surface magnetic moment. The remaining greater Co surface energy due to stronger interaction between less localized orbitals makes the Co GBs harder to separate.

Values of iCOHP measure bond strength. The Bi-Co bond at surface is weaker than Bi-Ni when magnetism is included (see Table IV) due to the fact that Bi is nonmagnetic and quenches the TM surface magnetic moments. All of these effects are greater at the Co surface than Ni due to Co's larger surface magnetic moments, 1.93$\mu_B$/atom compared with 0.78$\mu_B$/atom for Ni. This leads to a greater increase in Bi $\Delta H/A$ on Co(012) than Ni(012) surface, compared with the nonmagnetic case. This effect is also manifested from our COHP calculation that the Bi-Co bond is weakened by 0.12 eV, while Bi-Ni bond is weakened only by 0.02 eV due to magnetism. Thus Bi monolayers on Co(012) surface and Bi bilayers on Co Σ5(012) GB are less favorable to form than on Ni due to the stronger interaction between Co atoms than between Ni atoms resulting from greater localization of 3$d$ electrons on Ni, and weaker interaction between Bi and Co than between Bi and Ni, due to magnetism.

Apart from weaker interaction of Bi with Cu than with Ni, the Bi bilayer is less favorable on Cu than on Ni, since Bi gives electrons to Cu, increasing the filling of Cu $d$ states. This leads to stronger $d$ orbital antibonding among Cu atoms close to Bi rather than $s$ orbital antibonding as is inferred in

TABLE V. $\Delta F(T)/A$ of Bi bilayer at TM GBs; units are eV/Å$^2$. Values in parentheses are $\Delta H/A$.

| GB | Co | Ni | Cu |
|---|---|---|---|
| Σ 3(111) | 0.089(0.099) | 0.037(0.045) | 0.030(0.040) |
| Σ 5(120) | 0.012(0.004) | −0.043(−0.054) | −0.005(−0.009) |

[35]. Our COHP calculation results are shown in Fig. 6 (note that for Cu, unlike Co and Ni, antibonding states lie below bonding states at the equilibrium lattice constant). The Ni-Ni and Co-Co bonds close to Bi however are stronger than in the bulk, where no antibonds appear.

### D. Vibrational free energies

To incorporate the vibrational free energy we add $\Delta F_{\rm vib}$ to $\Delta H$, where the vibrational free energy $\Delta F_{\rm vib}$ is calculated from the phonon density of states within the harmonic approximation [36] by integrating over the contribution of all independent phonon modes. For a single phonon mode with vibrational frequency $\omega$, the vibrational free energy is $k_B T \ln[2\sinh(\hbar\omega/2k_B T)]$. The full vibrational free energy is

$$F_{\rm vib}(T) = k_B T \int g(\omega)\ln[2\sinh(\hbar\omega/2k_B T)]d\omega. \quad (5)$$

The phonon density of states $g(\omega)$ is calculated by employing the force constant method for phonon calculations with a similar method to [37]. In our study, we calculate the vibrational free energy of the Bi atoms while keeping the TM atoms fixed. The change of vibrational free energy by mixing can be calculated by

$$\Delta F_{\rm vib}(T)/A = \left[F_{\rm vib}^{\rm Bi\ film}(T) - F_{\rm vib}^{\rm Bi\ bulk}(T)\right]/A, \quad (6)$$

where the $F_{\rm vib}^{\rm Bi\ film}$ is the total vibrational free energy of Bi bilayer at TM grain, and $F_{\rm vib}^{\rm Bi\ bulk}$ is the vibrational free energy of Bi in bulk form. The total change of free energy by mixing is thus

$$\Delta F(T)/A = [\Delta H + \Delta F_{\rm vib}(T)]/A. \quad (7)$$

The results of Bi bilayer at TM GBs are shown in Table V. Vibrations leave the sign of $\Delta H$ unchanged for these GBs.

## IV. CONCLUSION

In conclusion, we have studied Bi segregation at Co, Ni, and Cu low energy Σ3(111) and high energy Σ5(120) GBs using density functional theory. Our results reproduce the experimental result that Bi does not form film at all Fe GBs but forms a bilayer film ubiquitously at Ni high energy GBs, and in a much narrower chemical potential window at Cu high energy GB. The difference between these metals can be explained by the localization of 3$d$ orbitals and also the loss of magnetism near the GB of Co (and presumably Fe). Moreover, Bi on Cu GB also increases the strength of antibonding, as confirmed by COHP calculation. We propose a model to predict the stability of Bi bilayer at various Ni GBs. Combining with the EAM GB energies from Ref. [33], the model suggests Bi bilayer is not thermodynamically stable on (111) twist CSL GBs but should be stable in most (100) twist CSL GBs.

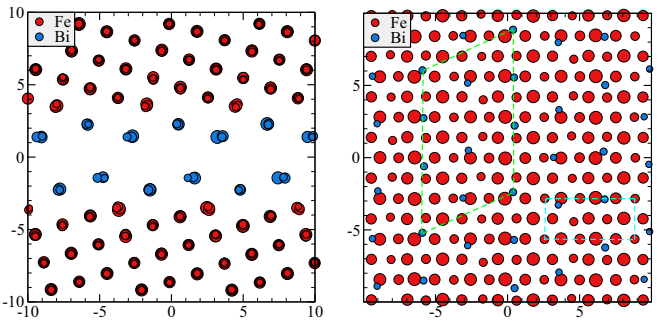


FIG. 7. (Color online) Side view (left) of relaxed Bi bilayer at Fe Σ5(012) GB and top view (right) of Bi monolayer on one side of the GB plane. The cyan cell is the Fe GB unit cell; the green cell is the Bi segregated GB unit cell. Atom size indicates depth (large below small). Length units are in Å.

## ACKNOWLEDGMENTS

The authors thank Jian Luo, Jeffrey Rickman, Zhiyang Yu, Anthony Rollett, Gregory Rohrer, and Martin Harmer for helpful discussion. Financial support from the ONR-MURI under Grant No. N00014-11-1-0678 is gratefully acknowledged.

## APPENDIX

### 1. Bi bilayer on Fe Σ5(012) GB

We calculated Bi bilayer enthalpy on Fe Σ5(012), a high energy GB which is created by cleaving the BCC bulk along the (012) plane and rotating one grain around [001] by 53.1° and rejoining the two parts. Our calculated GB energy is 0.098 eV/Å$^2$, close to the GB energy 0.104 eV/Å$^2$ of the lowest

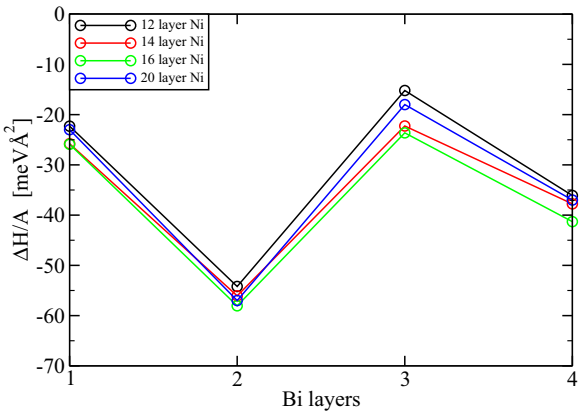


FIG. 8. (Color online) Convergence with respect to the number of Ni layers in calculation of Bi bilayer at Ni Σ5(210) GB. $\Delta H$ oscillates for different slab thickness due to the quantum size effect [39] which is less than 0.005 eV/ Å$^2$ for 1, 2, and 4 layer Bi films. For the trilayer Bi film, the oscillation is exaggerated by the fact that the trilayer structure is not stable. The 12 layer Ni slab is thus thick enough for our study that concentrates on monolayer and bilayer films.

energy structure in the literature [38]. We first studied Bi monolayers on Fe (012) surfaces and then calculated bilayer films on the GB with the stable surface structure at two sides of the GB plane. We used 10 layers of Fe at each side of the Bi film. The relaxed structure is shown in Fig. 7. The lowest $\Delta H/A$ is $+0.017$ eV/Å$^2$ and including vabriations as in Eqs. (5) and (7) the $\Delta F/A$ is $+0.016$ eV/Å$^2$ at 1000 K for bilayer films, which are large and positive indicating that the Bi bilayer is not stable even on this high energy GB.

### 2. Convergence with respect to number of Ni layers

Figure 8 depicts convergence with respect to the number of Ni layers.


[1] C. Scott, M. Kaliszewski, C. Greskovich, and L. Levinson, J. Am. Ceram. Soc. **85**, 1275 (2002).
[2] J. Cho, M. Harmer, H. Chan, J. Rickman, and A. Thompson, J. Am. Ceram. Soc. **80**, 1013 (1997).
[3] B. Joseph, M. Picat, and F. Barbier, Eur. Phys. J.: Appl. Phys. **5**, 19 (1999).
[4] K. Wolski and V. Laporte, Mater. Sci. Eng., A **495**, 138 (2008).
[5] R. Viswanadham, T. Sun, and J. Green, Metall. Mater. Trans. A **11**, 85 (1980).
[6] S. Knight, N. Birbilis, B. Muddle, A. Trueman, and S. Lynch, Corros. Sci. **52**, 4073 (2010).
[7] M. Tang, W. C. Carter, and R. M. Cannon, Phys. Rev. Lett. **97**, 075502 (2006).
[8] M. Harmer, Science **332**, 182 (2011).
[9] P. R. Cantwell, M. Tang, S. J. Dillon, J. Luo, G. S. Rohrer, and M. P. Harmer, Acta Mater. **62**, 1 (2014).
[10] S. J. Dillon, M. Tang, W. C. Carter, and M. P. Harmer, Acta Mater. **55**, 6208 (2007).
[11] J. Luo, H. Cheng, K. M. Asl, C. Kiely, and M. Harmer, Science **333**, 1730 (2011).
[12] A. Kundu, K. M. Asl, J. Luo, and M. P. Harmer, Scr. Mater. **68**, 146 (2013).
[13] J. Luo (private communication).
[14] J. Kang, G. C. Glatzmaier, and S.-H. Wei, Phys. Rev. Lett. **111**, 055502 (2013).
[15] R. Dronskowski and P. E. Bloechl, J. Phys. Chem. **97**, 8617 (1993).
[16] O. Jepsen and O. Andersen, Z. Phys. B: Condens. Matter **97**, 35 (1995).
[17] Q. Gao and M. Widom, Phys. Rev. B **88**, 155416 (2013).
[18] P. E. Blochl, Phys. Rev. B **50**, 17953 (1994).
[19] G. Kresse and D. Joubert, Phys. Rev. B **59**, 1758 (1999).
[20] J. P. Perdew, K. Burke, and M. Ernzerhof, Phys. Rev. Lett. **77**, 3865 (1996).
[21] G. Kresse and J. Hafner, Phys. Rev. B **47**, 558(R) (1993).
[22] G. Kresse and J. Furthmuller, Phys. Rev. B **54**, 11169 (1996).
[23] M. D. Sangid, H. Sehitoglu, H. J. Maier, and T. Niendorf, Mater. Sci. Eng., A **527**, 7115 (2010).
[24] V. L. E. Murr, *Interfacial Phenomena in Metal and Alloys* (Addison-Wesley, Redwood City, CA, 1975), p. 138.
[25] M. Yamaguchi, M. Shiga, and H. Kaburaki, J. Phys.: Condens. Matter **16**, 3933 (2004).
[26] M. A. Tschopp and D. L. Mcdowell, Philos. Mag. **87**, 3871 (2007).
[27] D. Kaminski, P. Poodt, E. Aret, N. Radenovic, and E. Vlieg, Surf. Sci. **575**, 233 (2005).
[28] B. Blum and H. Ascolani, Surf. Sci. **482–485**, 946 (2001).
[29] J. R. Kitchin, K. Reuter, and M. Scheffler, Phys. Rev. B **77**, 075437 (2008).
[30] C. Panja, M. E. Jones, J. M. Heitzinger, S. C. Gebhard, and B. E. Koel, J. Phys. Chem. B **104**, 3130 (2000).
[31] T. R. J. Bollmann, R. van Gastel, H. J. W. Zandvliet, and B. Poelsema, Phys. Rev. Lett. **107**, 176102 (2011).
[32] E. A. Holm, D. L. Olmsted, and S. M. Foiles, Scr. Mater. **63**, 905 (2010).
[33] D. L. Olmsted, S. M. Foiles, and E. A. Holm, Acta Mater. **57**, 3694 (2009).
[34] R. Schweinfest, A. Paxton, and M. W. Finnis, Nature (London) **432**, 1008 (2004).
[35] G. Duscher, M. F. Chisholm, U. Alber, and M. Ruhle, Nat. Mater. **3**, 621 (2004).
[36] G. Kresse, J. Furthmüller, and J. Hafner, Europhys. Lett. **32**, 729 (1995).
[37] M. Mihalkovič and M. Widom, Phys. Rev. B **85**, 014113 (2012).
[38] T. Ossowski, J. Kuriplach, E. Zhurkin, M. Hou, and A. Kiejna, 27th Max Born Symposium, Wroclaw, Poland, 2010, URL http://www.ift.uni.wroc.pl/mborn27/download/files/SessionX_3_Ossowski.pdf
[39] B. Sun, P. Zhang, S. Duan, X.-G. Zhao, and Q.-K. Xue, Phys. Rev. B **75**, 245422 (2007).